A Large-scale Comparison of Cortical and Subcortical Structural Segmentation Methods in Alzheimer's Disease: a Statistical Approach

Jafar Zamani[1], Ali Sadr[1,*], Amir-Homayoun Javadi[2,3,4,*]

[1]School of Electrical Engineering, Iran University of Science and Technology, Tehran, Iran
[2]School of Psychology, University of Kent, Canterbury, UK
[3]Institute of Behavioural Neuroscience, University College London, London, UK
[4]School of Rehabilitation, Tehran University of Medical Sciences, Tehran, Iran

Running title: Structural Segmentation in Alzheimer's Disease

[*]**Corresponding authors:**

Ali Sadr
Address: School of Electrical Engineering,
Iran University of Science & Technology,
Narmak, Tehran, Iran
Phone: +98 21 7322 5757
E-Mail: sadr@iust.ac.ir

Amir-Homayoun Javadi
Address: School of Psychology, Keynes College
University of Kent
Canterbury, UK
Phone: +44 1227 827 770
E-Mail: a.h.javadi@gmail.com

Abstract

Background. Alzheimer's disease (AD) is a neurodegenerative disease that leads to anatomical atrophy, as evidenced by magnetic resonance imaging (MRI). Automated segmentation methods are developed to help with the segmentation of different brain areas. However, their reliability has yet to be fully investigated. To have a more comprehensive understanding of the distribution of changes in AD, as well as investigating the reliability of different segmentation methods, in this study we compared volumes of cortical and subcortical brain segments, using automated segmentation methods in more than 60 areas between AD and healthy controls (HC).

Methods. A total of 44 MRI images (22 AD and 22 HC, 50% females) were taken from the minimal interval resonance imaging in Alzheimer's disease (MIRIAD) dataset. HIPS, volBrain, CAT and BrainSuite segmentation methods were used for the subfields of hippocampus, and the rest of the brain.

Results. While HIPS, volBrain and CAT showed strong conformity with the past literature, BrainSuite misclassified several brain areas. Additionally, the volume of the brain areas that successfully discriminated between AD and HC showed a correlation with mini mental state examination (MMSE) scores. The two methods of volBrain and CAT showed a very strong correlation. These two methods, however, did not correlate with BrainSuite.

Conclusion. Our results showed that automated segmentation methods HIPS, volBrain and CAT can be used in the classification of AD and HC. This is an indication that such methods can be used to inform researchers and clinicians of underlying mechanisms and progression of AD.

Keywords: volumetric MRI T1, atrophy, automatic segmentation, dementia, volBrain, CAT, BrainSuite, HIPS

1 Introduction

Alzheimer's disease (AD) is a devasting neurodegenerative disease, contributing to 60-70% of dementia cases [1]. Currently there are around 50 million people with dementia worldwide. In 2015, the total global societal cost of dementia was estimated to be US$ 818 billion [2,3]. Mainly due to increased life-expectancy, the total number of people with dementia is projected to reach 82 million (64% increase) in 2030, with between 49 and 57 million of these cases being AD [4]. Whilst several drugs are available to mitigate the symptoms in some cases, no treatments are available that prevent progression from the relatively late stage at which the disease is diagnosed [5].

AD is characterised by two main pathological hallmarks: extracellular amyloid deposits, composed of insoluble amyloid beta (Aβ) protein, and intra-neuronal neurofibrillary tangles (NFTs), containing hyperphosphorylated tau protein [6]. AD is also characterised by a significant loss of neurons and synapses, resulting in brain shrinkage and atrophy [7,8]. Structural changes have been shown to be one of the earliest biomarkers that can be used in the diagnosis of AD [9–11]. Much effort has been devoted to find patterns of changes in the structure of different brain areas that can be reliably used for diagnosis of AD [12].

Earlier investigations relied mostly on manual segmentation of brain areas requiring a great deal of expertise and time [13–16]. Therefore, the majority of the focus has been devoted to changes in the hippocampus due to its distinct structure [17]. It has been shown that a loss in hippocampal volume can be an indication of AD [18,19]. Further investigations have looked at subfields of the hippocampus, showing a nonuniform rate of neuroplasticity due to their specialisation [20–22]. For example, it has been shown that NFT begin in the medial temporal region and exhibit a characteristic distribution pattern across subfields, starting in the CA1 and later spreading to subiculum, CA2, CA3 and CA4/Dentate Gyrus [23–27].

With the development of semi- and fully-automated segmentation methods, however, it has now become easier and faster to segment not only the hippocampal area, but also other brain areas [28–32]. HIPpocampus subfield Segmentation (HIPS) [33], volBrain [34], Computational Anatomy Toolbox (CAT) [35,36], BrainSuite [37,38] and FreeSurfer [39] are some of the commonly used semi- and fully-automated methods. These methods, however, are yet under development [40,41]. For example, CA1 segmentation in the FreeSurfer v5.3 was partially included in the subiculum [18] potentially explaining why the CA1 field was reported to be insensitive to AD pathology in some [42,43] but not all [44,45]. Similar findings have recently raised questions and

concerns regarding the accuracy and consistency of these methods [46–49]. Therefore, it is important to investigate the accuracy of these methods further [50].

Benefiting from the computational power of automated methods, analysis of a large number of brain images has become more feasible. Large datasets of brain scans such as Minimal Interval Resonance Imaging in Alzheimer's Disease (MIRIAD), a public database of Alzheimer's magnetic resonance imaging (MRI) [51] , offer a great opportunity to have a more comprehensive approach to the underlying mechanism and progression of AD [52–56]. It also facilitates multisite studies to form a more accurate understanding of the disease [57,58].

Mini mental state examination (MMSE) is one of the commonly accepted measurements of cognitive ability, in particular in clinical settings [59–61]. This measure has been widely used in classification of AD. For example, MIRIAD classifies participants with score between 12 and 26/30 as AD and those higher than 26/30 as healthy control. There is huge body of literature showing correlation between MMSE score and brain atrophy [62–64].

The aim of this study was to investigate the reliability of four automated segmentation methods of volBrain, CAT and BrainSuite for segmentation of the whole brain, and HIPS for segmentation of subfields of hippocampus, which belongs to the same analysis tool as volBrain. We used images belonging to MIRIAD. Correlation of the volume of each brain area with MMSE scores are also investigated. To investigate the reliability of the three methods volBrain, CAT and BrainSuite, the correlation of their common brain areas is also reported.

2 Material and Methods

2.1 Subjects

We used 44 images (22 AD and 22 HC) taken from the Minimal Interval Resonance Imaging in Alzheimer's Disease (MIRIAD) dataset [51]. Table 1 shows a summary of the descriptives of the participants.

2.2 Magnetic Resonance Imaging (MRI)

Data was extracted from MIRIAD database. All subjects underwent MRI scanning on a 1.5 T Signa scanner (GE Medical Systems, Milwaukee, WI, USA). T1-weighted volumetric images were obtained using an inversion recovery prepared fast spoiled gradient echo sequence with acquisition parameters time to repetition = 15 ms, time to echo = 5.4 ms, flip angle = 15°, TI =

650 ms, a 24-cm field of view and a 256 × 256 matrix, to provide 124 contiguous 1.5-mm thick slices in the coronal plane (voxels 0.9735 × 0.9735 × 1.5 mm^3) [51].

2.3 Methods

HIPS and volBrain; The volumes of Cerebrospinal fluid (CSF), white matter (WM), grey matter (GM), brain hemispheres, cerebellum and brainstem were obtained using volBrain pipeline [34]. This method is based on an advanced pipeline providing automatic segmentation of different brain structures from T1 weighted MRI, Figure 1. The preprocessing is based on the following procedure: (1) a denoising step with an adaptive non-local mean filter, (2) an affine registration in the Montreal Neurological Institute (MNI) space, (3) a correction of the image inhomogeneities, and (4) an intensity normalisation. (5) Afterwards, MRI images are segmented in the MNI space using non-local patch-based multi-atlas method. Images were corrected for intensity inhomogeneity using the N4 algorithm [65], and the images were segmented into brain/non-brain using a semi-automated technique (MIDAS). The Non-Local Means filter [66] was applied to each pixel of the image by computing a weighted average of surrounding pixels using a robust similarity measure that takes into account the neighbouring pixels surrounding the pixel being compared. This segmentation method is based on the idea of non-local patch-based label fusion technique, where patches of the brain image to be segmented are compared with those of the training library, looking for similar patterns within a defined search volume to assign the proper label [67,68]. HIPS and volBrain are used for segmentation of the hippocampus subfields and the rest of the brain, respectively [33].

CAT; Computational Anatomy Toolbox (CAT) is a powerful package for brain T1-MRI data segmentation, Figure 2. It is a voxel base estimation method [69]. The CAT preprocessing steps are as follows: (1) spatial registration to a template, (2) tissue segmentation into grey, white matter and CSF, and (3) bias correction of intensity non-uniformities. (4) Finally, segments are extracted by scaling the amount of volume changes based on spatial registration, so that the total volume of grey matter in the modulated image remains the same as the original image. For correction of the orientation and size of the brain, non-linear registration methods are applied to the image [70]. Projection-based thickness (PBT) method is used for calculation of the cortical thickness and central surface [70,71]. Spatial-adaptive Non-Local Means (SANLM) and classical Markov Random Field (MRF) were used for image Denoising [72]. Adaptive Maximum a Posterior (AMAP) method was used for segmentation [69].

BrainSuite; BrainSuite is an open source software tool that enables largely automated cortical surface extraction from MRI of the brain, Figure 3. BrainSuite includes automatic cortical surface extraction, bias field correlation, cerebrum labelling, and surface generation features. Also, this toolbox is used in tractography and connectivity matrix calculation in diffusion imaging data [37].

2.4 Statistical Analysis

Independent-sample t-tests are run to compare the volume of different brain areas between the AD and HC groups for volBrain, CAT and BrainSuite for the whole brain, and HIPS for the hippocampus subfields. Bivariate-correlation analyses are also run to investigate the relationship between volume and MMSE scores for all four segmentation methods. Correlational analyses are run between the common brain areas in volBrain, CAT and BrainSuite to investigate the relationship between the three methods. Bonferroni correction is applied to account for multiple comparison.

3 Results

Using three automatic segmentation methods CAT, volBrain and BrainSuite, we segmented the whole brain, and using HIPS we segmented the hippocampus. Using independent-sample t-tests we compared the volumetric data for AD and HC for each segment. Figures 3-6 show sample output images for one AD patient and one HC participant. Furthermore, we investigated the correlation of volumetric data with MMSE scores in both groups.

CAT segmentation method returned data for 63 distinct brain areas. This method highlighted many brain areas that are significantly different between the two groups, Table 2. In particular fusiform gyrus, parahippocampal gyrus, hippocampus, entorhinal cortex, amygdala, temporal gyri, thalamus, nucleus accumbens, insula, caudate and precuneus were significantly different. Importantly, the size of all these brain areas showed a strong correlation with MMSE scores. For further details see supplementary figures 1-3.

=== Table 2 ===

=== Figure 4 ===

volBrain segmentation method returned data for eight distinct brain areas. In particular the amygdala, hippocampus, nucleus accumbens, thalamus and caudate were significantly

different between the two groups, Table 3. Again, the size of all these brain areas showed a strong correlation with MMSE scores. For further details see supplementary figures 4-6.

=== Table 3 ===

=== Figure 5 ===

BrainSuite segmentation method returned data for 50 distinct brain areas. In contrast to CAT and volBrain, this method highlighted only six brain areas that are significantly different between the two groups, Table 4. These brain areas included temporal gyri, third ventricle, supramarginal gyrus and angular gyrus. Similar to previous segmentation methods, all these brain areas showed strong correlation with MMSE scores. For further details see supplementary figures 7-9.

=== Table 4 ===

=== Figure 6 ===

HIPS segmentation method returned data for the whole hippocampus and five of its subfields: CA1, CA2-CA3, CA4/Dentate Gyrus, Subiculum and strata radiatum/lacunosum/moleculare (SR-SL-SM). All these areas showed a significant difference between the two groups, Table 5. The size of hippocampus and all its subfields showed strong correlation with MMSE scores. For further details see supplementary figures 10-12.

=== Table 5 ===

=== Figure 7 ===

To investigate the relationship between the three whole-brain segmentation methods CAT, volBrain and BrainSuite, we ran correlational analysis, Table 6. Seven brain areas were common between these methods: nucleus accumbens, amygdala, caudate, globus pallidus, hippocampus, putamen and thalamus. CAT and volBrain showed strong correlation for nucleus accumbens, amygdala, caudate, hippocampus and thalamus. Two brain areas globus pallidus and putamen were not significantly correlated. These brain areas did not show significant difference between the two groups either. BrainSuite, however, showed no significant correlation with either of the other two segmentation methods.

=== Table 6 ===

4 Discussion

We used HIPS automated method to segment the subfields of hippocampus, and CAT, volBrain and BrainSuite automated methods to segment the whole brain using T1 weighted MRI data. Our results showed that all subfields of hippocampus in the Alzheimer's Disease (AD) group were significantly smaller than those of the healthy control (HC) group. The atrophy of all subcomponents of hippocampus were correlated with the MMSE measure. Quite a large portion of cortical and subcortical areas in the brain were also smaller in the AD group as compared to the control group, as evident from CAT and volBrain segmentation results. The shrinkage in these brain areas mostly showed a strong correlation with MMSE measure. BrainSuite failed to discriminate between the two groups. While CAT and volBrain shows a strong correlation, BrainSuite did not show any significant correlation with CAT and volBrain.

With the advancement of computational methods, fine-grain analysis of the brain areas is more feasible [73–75]. Earlier methods relied heavily on manual segmentation of the brain areas, which was extremely time demanding and also required a great level of expertise. Therefore, the majority of the analysis was limited to brain areas with more distinct structure, such as the hippocampus. Many semi- and fully-automated segmentation methods have been developed. While these methods have been used more commonly in recent years, the reliability and accuracy of these methods was yet to be fully studied. We used four pipelines of HIPS [33], volBrain [34], CAT [35,36] and BrainSuite [37]. In this study we evaluated their reliability by looking at their ability to discriminate between AD and HC groups, whether a correlation existed between them, their correlation with MMSE scores, and comparing their results with past literature. Our results showed strong reliability of HIPS, volBrain and CAT. These methods have been successfully applied to brain images from those with AD [76–79].

BrainSuite, however, underperformed greatly. For example, it failed to accurately segment the hippocampus, thalamus and amygdala to show a significant difference between the two groups. While this automatic segmentation method has been used frequently in past research [80], its application has been mostly limited to the processing of brains with no atrophy [81,82], as well as detection of gross segments such as tumours [83]. This highlights the importance of validation studies such as ours to gain a greater understanding of the applications and limitations of different methods [84–87].

The volume of the hippocampus is considered as an important biomarker for AD and has been included in recently proposed research diagnostic criteria [88,89]. It has been shown that the

hippocampal atrophy estimated on anatomical T1 weighted MRI can help in classifying the different stages of AD [90–92]. Confirming past literature, our results showed that the hippocampus volume significantly differed between AD and the control group.

Histological studies have shown that lesions are not uniformly distributed within the hippocampus [91,93]. Neuronal loss results in a reduction of the thickness of the layers richer in neuronal bodies, while the loss of synapses results in the reduction of the layers poorer in neuronal bodies [94–97] and these changes are stage-dependent [98,99]. Our results, however, failed to differentiate the contribution of these subfields in AD; they all showed significant reduction in size, compared to the control group. This effect could be because our AD group consisted of those with later stages of AD. The contribution of different subfields of the hippocampus is more visible in those with mild cognitive impairment [100–102]. Therefore, in future studies it would be informative to include participants with different stages of AD to investigate the contribution of different subfields of the hippocampus in AD.

While the contribution of atrophy in the hippocampus has been widely studied, the role of atrophy in the rest of the brain in AD is less clear [40]. An important contributing factor is that the boundaries of the hippocampus are easier for human operators or automated algorithms to recognise than other brain areas such as the amygdala, entorhinal cortex or thalamus [40]. Due to methodological advances, however, it is now possible to measure atrophy across the entire cortex with good precision [103]. Our results from CAT and volBrain methods showed strongly significant differences between many brain areas such as the amygdala, thalamus, nucleus accumbens, insula and caudate. These findings are in-line with past literature showing similar differences in these brain areas [40,104–106].

There is a growing body of literature showing a correlation between cognitive decline and brain atrophy [62,107,108]. For example, it has been shown that basal forebrain changes are correlated with cognitive decline in MCI and AD patients, as measured with recall task and MMSE [109,110], as well as healthy participants that later progressed to AD [111]. Atrophy of other brain areas such as lateral and medial parietal cortex, as well as lateral temporal cortex have also been shown to have a correlation with cognitive decline [112]. Our results showed a strong correlation between brain atrophy and cognitive decline as measured by MMSE. All brain areas that were significantly different between the AD and the control group showed a significant correlation with MMSE, except for the caudate (CAT $p = 0.001155$, volBrain $p = 0.005091$, Bonferroni corrected statistic not significant). While the effect of shrinkage of the caudate in AD is not very clear [113], there is some evidence that caudate volume has a correlation with MMSE

measures, although not as strongly as other brain areas such as the thalamus [63,114]. An important consideration is that atrophy in the left caudate has a stronger role in AD, as compared to the right caudate [113,115]. Our analysis combined both the left and right caudate, which may have led to this inconsistency between our results and previous literature.

Although AD commonly presents as an amnestic syndrome, there is significant heterogeneity across individuals [116], which is accompanied by different atrophy patterns [64,117–119]. For example, while those with more language difficulties might exhibit greater atrophy in temporal or parietal regions [120,121], those with more visual difficulties might have greater atrophy in posterior cortical regions [122,123]. Availability of the automated systems offers many opportunities, such as the ability to analyse a large number of brain images with reasonable time and expertise. This is in particular very appealing, considering the increased number of large datasets such as MIRIAD. Automated systems can go through the collection and aggregate data from a wide range of participants, healthy and patients to gain a greater understanding of AD. This is important considering the heterogeneity of the disease and its progression [124].

Another application of automated systems is in clinical settings. By the time of diagnosis, rapid ongoing atrophy is already far advanced [125,126]. Early diagnosis of AD can help with deceleration of the progression of the disease [21,127,128]. This is particularly important as there are modifiable factors that can help with brain health[129–131]. Therefore, a massive effort has been devoted to the development of diagnostic methods to enable researchers and clinicians to detect AD and cases with potential progression to AD, as early as possible [132,133]. For the development of preventive strategies, it is important to predict future brain atrophy, as this may aid in identifying which individuals with normal cognition are more susceptible of progressing to later stages of AD [134–136]. Automated systems provide additional information to clinicians, enabling them to have a greater understanding of the progression of the atrophy [12,137]. Some of these methods have already received approval from different licensing bodies such as CE (European conformity) and FDA (food and drug administration, USA) approval [138]. These methods, however, come with some limitations such as speed of processing, expensive licences, or requirement of other specialised software. This study is another step to evaluate freely available analytical tools to achieve an ideal analysis pipeline, suitable for researchers and clinicians.

Availability of the reliable automated segmentation methods enables researchers and clinicians to have a greater understanding of the underlying mechanisms and the progression of the AD.

This will allow them to attempt to prevent or decelerate the progression of the disease more effectively. Future research can look at the rate of atrophy to predict the progression of disease [139–142]. This rate can be helpful to have a more informed understanding whether an individual with MCI will later progress to AD or not [105,143,144]. The output of automated segmentation methods can also be used in training of intelligent classification methods such as those using artificial neural networks and support vector machines, which has shown promising results [145–154].

The purpose of this article was not to identify the superiority of any particular automatic segmentation method over another, but to solely highlight possible limitations and applications of four commonly used segmentation methods. We proposed that CAT, volBrain and HIPS are methods that can robustly operate on brain images with significant atrophy and can be used in research and clinical settings. BrainSuite, however, should be used with caution for brain images with atrophy.

Authors' Contribution

JZ and AHJ analysed the data. JZ and AHJ wrote the manuscript. JZ, AHJ and AS revised the manuscript.

References

1. Scheltens, P. *et al.* Alzheimer's disease. *The Lancet* **388**, 505–517 (2016).
2. World Health Organization. *Fact Sheet-Dementia*. (2015).
3. Association, A. 2019 Alzheimer's disease facts and figures. *Alzheimer's & Dementia* **15**, 321–387 (2019).
4. Nichols, E. *et al.* Global, regional, and national burden of Alzheimer's disease and other dementias, 1990–2016: a systematic analysis for the Global Burden of Disease Study 2016. *The Lancet Neurology* **18**, 88–106 (2019).
5. Knapp, M. *et al.* Cost-effectiveness of donepezil and memantine in moderate to severe Alzheimer's disease (the DOMINO-AD trial). *International Journal of Geriatric Psychiatry* **32**, 1205–1216 (2017).

6. Montine, T. J. *et al.* National institute on aging-Alzheimer's association guidelines for the neuropathologic assessment of Alzheimer's disease: A practical approach. *Acta Neuropathologica* **123**, 1–11 (2012).

7. Duyckaerts, C., Delatour, B. & Potier, M. C. Classification and basic pathology of Alzheimer disease. *Acta Neuropathologica* **118**, 5–36 (2009).

8. Edwards, F. A. A Unifying Hypothesis for Alzheimer's Disease: From Plaques to Neurodegeneration. *Trends in Neurosciences* **42**, 310–322 (2019).

9. McConathy, J. & Sheline, Y. I. Imaging biomarkers associated with cognitive decline: A review. *Biological Psychiatry* **77**, 685–692 (2015).

10. Tabatabaei-Jafari, H., Shaw, M. E. & Cherbuin, N. Cerebral atrophy in mild cognitive impairment: A systematic review with meta-analysis. *Alzheimer's and Dementia: Diagnosis, Assessment and Disease Monitoring* **1**, 487–504 (2015).

11. Grundman, M. *et al.* Mild Cognitive Impairment Can Be Distinguished from Alzheimer Disease and Normal Aging for Clinical Trials. *Archives of Neurology* **61**, 59–66 (2004).

12. Frisoni, G. B., Fox, N. C., Jack, C. R., Scheltens, P. & Thompson, P. M. The clinical use of structural MRI in Alzheimer disease. *Nature Reviews Neurology* **6**, 67–77 (2010).

13. Mueller, S. G. *et al.* Hippocampal atrophy patterns in mild cognitive impairment and alzheimer's disease. *Human Brain Mapping* **31**, 1339–1347 (2010).

14. Kerchner, G. A. *et al.* Hippocampal CA1 apical neuropil atrophy in mild Alzheimer disease visualized with 7-T MRI. *Neurology* **75**, 1381–1387 (2010).

15. Yassa, M. A. *et al.* High-resolution structural and functional MRI of hippocampal CA3 and dentate gyrus in patients with amnestic Mild Cognitive Impairment. *NeuroImage* **51**, 1242–1252 (2010).

16. Adachi, M. *et al.* Morphology of the inner structure of the hippocampal formation in Alzheimer disease. *American Journal of Neuroradiology* **24**, 1575–1581 (2003).

17. McRae-McKee, K. *et al.* Combining hippocampal volume metrics to better understand Alzheimer's disease progression in at-risk individuals. *Scientific Reports* **9**, 1–9 (2019).

18. de Flores, R., la Joie, R. & Chételat, G. Structural imaging of hippocampal subfields in healthy aging and Alzheimer's disease. *Neuroscience* **309**, 29–50 (2015).

19. Nobis, L. *et al.* Hippocampal volume across age: Nomograms derived from over 19,700 people in UK Biobank. *NeuroImage: Clinical* **23**, 101904 (2019).

20. Mueller, S. G. & Weiner, M. W. Selective effect of age, Apo e4, and Alzheimer's disease on hippocampal subfields. *Hippocampus* **19**, 558–564 (2009).

21. Nestor, P. J., Scheltens, P. & Hodges, J. R. Advances in the early detection of Alzheimer's disease. *Nature Medicine* **10**, S34–S41 (2004).

22. Wisse, L. E. M. *et al.* Hippocampal subfield volumes at 7T in early Alzheimer's disease and normal aging. *Neurobiology of Aging* **35**, 2039–2045 (2014).

23. Braak, H. & Braak, E. Alzheimer's disease affects limbic nuclei of the thalamus. *Acta Neuropathologica* **81**, 261–268 (1991).

24. Bobinski, M. *et al.* Relationships between Regional Neuronal Loss and Neurofibrillary Changes in the Hippocampal Formation and Duration and Severity of Alzheimer Disease. *Journal of Neuropathology and Experimental Neurology* **56**, 414–420 (1997).

25. Schönheit, B., Zarski, R. & Ohm, T. G. Spatial and temporal relationships between plaques and tangles in Alzheimer-pathology. *Neurobiology of Aging* **25**, 697–711 (2004).

26. Li, F., Ball, S., Katz, B. & Smith, A. Case report of syncope during a transcranial direct current stimulation experiment in a healthy adult participant. *Brain Stimulation* **0**, 1201–1202 (2018).

27. la Joie, R. *et al.* Hippocampal subfield volumetry in mild cognitive impairment, Alzheimer's disease and semantic dementia. *NeuroImage: Clinical* **3**, 155–162 (2013).

28. Litjens, G. *et al.* A survey on deep learning in medical image analysis. *Medical Image Analysis* **42**, 60–88 (2017).

29. Han, X. *et al.* Reliability of MRI-derived measurements of human cerebral cortical thickness: The effects of field strength, scanner upgrade and manufacturer. *NeuroImage* **32**, 180–194 (2006).

30. Ambarki, K., Wåhlin, A., Birgander, R., Eklund, A. & Malm, J. MR imaging of brain volumes: Evaluation of a fully automatic software. *American Journal of Neuroradiology* **32**, 408–412 (2011).

31. Kerchner, G. A. *et al.* Shared vulnerability of two synaptically-connected medial temporal lobe areas to age and cognitive decline: A seven tesla magnetic resonance imaging study. *Journal of Neuroscience* **33**, 16666–16672 (2013).

32. Yushkevich, P. A. *et al.* Automated volumetry and regional thickness analysis of hippocampal subfields and medial temporal cortical structures in mild cognitive impairment. *Human Brain Mapping* **36**, 258–287 (2015).

33. Romero, J. E., Coupé, P. & Manjón, J. v. HIPS: A new hippocampus subfield segmentation method. *NeuroImage* **163**, 286–295 (2017).

34. Manjón, J. v. & Coupé, P. Volbrain: An online MRI brain volumetry system. *Frontiers in Neuroinformatics* **10**, 1–14 (2016).

35. Tzourio-Mazoyer, N. *et al.* Automated Anatomical Labeling of Activations in SPM Using a Macroscopic Anatomical Parcellation of the MNI MRI Single-Subject Brain. *NeuroImage* **15**, 273–289 (2002).

36. Rolls, E. T., Huang, C.-C., Lin, C.-P., Feng, J. & Joliot, M. Automated anatomical labelling atlas 3. *NeuroImage* **206**, 116189 (2020).

37. Shattuck, D. W. & Leahy, R. M. BrainSuite: An automated cortical surface identification tool. *Medical Image Analysis* **6**, 129–142 (2002).

38. Shattuck, D. W. *et al.* Semi-automated method for delineation of landmarks on models of the cerebral cortex. *Journal of Neuroscience Methods* **178**, 385–392 (2009).

39. Yushkevich, P. A. *et al.* Nearly automatic segmentation of hippocampal subfields in in vivo focal T2-weighted MRI. *NeuroImage* **53**, 1208–1224 (2010).

40. Pini, L. *et al.* Brain atrophy in Alzheimer's Disease and aging. *Ageing Research Reviews* **30**, 25–48 (2016).

41. Bigler, E. D. *et al.* FreeSurfer 5.3 versus 6.0: are volumes comparable? A Chronic Effects of Neurotrauma Consortium study. *Brain Imaging and Behavior* (2018) doi:10.1007/s11682-018-9994-x.

42. Kook Lim, H. *et al.* Automated hippocampal subfields segmentation in late life depression. *Journal of Affective Disorders* **143**, 253–256 (2012).

43. Hanseeuw, B. J. *et al.* Mild cognitive impairment: Differential atrophy in the hippocampal subfields. *American Journal of Neuroradiology* **32**, 1658–1661 (2011).

44. Li, Y. di, Dong, H. B., Xie, G. M. & Zhang, L. J. Discriminative analysis of mild alzheimer's disease and normal aging using volume of hippocampal subfields and hippocampal mean diffusivity: An in vivo magnetic resonance imaging study. *American Journal of Alzheimer's Disease and other Dementias* **28**, 627–633 (2013).

45. Khan, U. A. *et al.* Molecular drivers and cortical spread of lateral entorhinal cortex dysfunction in preclinical Alzheimer's disease. *Nature Neuroscience* **17**, 304–311 (2014).

46. Wisse, L. E. M., Biessels, G. J. & Geerlings, M. I. A Critical Appraisal of the Hippocampal Subfield Segmentation Package in FreeSurfer. *Frontiers in Aging Neuroscience* **6**, 127–134 (2014).

47. Cover, K. S., van Schijndel, R. A., Bosco, P., Damangir, S. & Redolfi, A. Can measuring hippocampal atrophy with a fully automatic method be substantially less noisy than manual segmentation over both 1 and 3 years? *Psychiatry Research - Neuroimaging* **280**, 39–47 (2018).

48. Marizzoni, M. *et al.* Longitudinal reproducibility of automatically segmented hippocampal subfields: A multisite European 3T study on healthy elderly. *Human Brain Mapping* **36**, 3516–3527 (2015).

49. Bender, A. R. *et al.* Optimization and validation of automated hippocampal subfield segmentation across the lifespan. *Human Brain Mapping* **39**, 916–931 (2018).

50. Pantazis, D. *et al.* Comparison of landmark-based and automatic methods for cortical surface registration. *NeuroImage* **49**, 2479–2493 (2010).

51. Malone, I. B. *et al.* MIRIAD-Public release of a multiple time point Alzheimer's MR imaging dataset. *NeuroImage* **70**, 33–36 (2013).

52. Iglesias, J. E. *et al.* Bayesian longitudinal segmentation of hippocampal substructures in brain MRI using subject-specific atlases. *NeuroImage* **141**, 542–555 (2016).

53. Cash, D. M. *et al.* Assessing atrophy measurement techniques in dementia: Results from the MIRIAD atrophy challenge. *NeuroImage* **123**, 149–164 (2015).

54. Platero, C., Lin, L. & Tobar, M. C. Longitudinal Neuroimaging Hippocampal Markers for Diagnosing Alzheimer's Disease. *Neuroinformatics* **17**, 43–61 (2019).

55. Giraldo, D. L., García-Arteaga, J. D., Cárdenas-Robledo, S. & Romero, E. Characterization of brain anatomical patterns by comparing region intensity distributions: Applications to the description of Alzheimer's disease. *Brain and Behavior* **8**, 1–11 (2018).

56. Ardekani, B. A., Convit, A. & Bachman, A. H. Analysis of the MIRIAD Data Shows Sex Differences in Hippocampal Atrophy Progression. *Journal of Alzheimer's Disease* **50**, 847–857 (2016).

57. Carrillo, M. C., Bain, L. J., Frisoni, G. B. & Weiner, M. W. Worldwide Alzheimer's disease neuroimaging initiative. *Alzheimer's and Dementia* **8**, 337–342 (2012).

58. van Horn, J. D. & Toga, A. W. Multisite neuroimaging trials. *Current Opinion in Neurology* **22**, 370–378 (2009).

59. Schneider, L. S. & Goldberg, T. E. Composite cognitive and functional measures for early stage Alzheimer's disease trials. *Alzheimer's & Dementia: Diagnosis, Assessment & Disease Monitoring* **12**, 1–9 (2020).

60. Dicks, E. *et al.* Modeling grey matter atrophy as a function of time, aging or cognitive decline show different anatomical patterns in Alzheimer's disease. *NeuroImage: Clinical* **22**, 101786 (2019).

61. Folstein, M. F., Folstein, S. E. & McHugh, P. R. "Mini-mental state": a practical method for grading the cognitive state of patients for the clinician. *Journal of psychiatric research* **12**, 189–198 (1975).

62. Nelson, P. T. *et al.* Correlation of Alzheimer Disease Neuropathologic Changes With Cognitive Status: A Review of the Literature. *Journal of Neuropathology & Experimental Neurology* **71**, 362–381 (2012).

63. Ferrarini, L. *et al.* MMSE scores correlate with local ventricular enlargement in the spectrum from cognitively normal to Alzheimer disease. *NeuroImage* **39**, 1832–1838 (2008).

64. Risacher, S. L. *et al.* Alzheimer disease brain atrophy subtypes are associated with cognition and rate of decline. *Neurology* **89**, 2176–2186 (2017).

65. Tustison, N. J. *et al.* N4ITK: Improved N3 bias correction. *IEEE Transactions on Medical Imaging* **29**, 1310–1320 (2010).

66. Manjón, J. v., Coupé, P., Martí-Bonmatí, L., Collins, D. L. & Robles, M. Adaptive non-local means denoising of MR images with spatially varying noise levels. *Journal of Magnetic Resonance Imaging* **31**, 192–203 (2010).

67. Coupé, P. *et al.* Patch-based segmentation using expert priors: Application to hippocampus and ventricle segmentation. *NeuroImage* **54**, 940–954 (2011).

68. Romero, J. E., Manjón, J. v., Tohka, J., Coupé, P. & Robles, M. NABS: Non-local automatic brain hemisphere segmentation. *Magnetic Resonance Imaging* **33**, 474–484 (2015).

69. Ashburner, J. & Friston, K. J. Unified segmentation. *NeuroImage* **26**, 839–851 (2005).

70. Gaser, C., & Dahnke, R. *CAT-A Computational Anatomy Toolbox for the Analysis of Structural MRI Data*. *Human Brain Mapping* (2016).

71. Dahnke, R. & Gaser, C. *Brain structural trajectories over the adult lifespan*. *Human Brain Mapping* (2017).

72. Manjón, J. v., Coupé, P., Martí-Bonmatí, L., Collins, D. L. & Robles, M. Adaptive non-local means denoising of MR images with spatially varying noise levels. *Journal of Magnetic Resonance Imaging* **31**, 192–203 (2010).

73. Brewer, J. B., Magda, S., Airriess, C. & Smith, M. E. Fully-automated quantification of regional brain volumes for improved detection of focal atrophy in Alzheimer disease. *American Journal of Neuroradiology* **30**, 578–580 (2009).

74. Hata, K. *et al.* Automated Volumetry of Medial Temporal Lobe Subregions in Mild Cognitive Impairment and Alzheimer Disease. *Alzheimer Disease and Associated Disorders* **33**, 206–211 (2019).

75. Fischl, B. *et al.* Whole brain segmentation: Automated labeling of neuroanatomical structures in the human brain. *Neuron* **33**, 341–355 (2002).

76. Haeger, A. *et al.* Effect of a multicomponent exercise intervention on brain metabolism: A randomized controlled trial on Alzheimer's pathology (Dementia-MOVE). *Alzheimer's & Dementia: Translational Research & Clinical Interventions* **6**, 1–9 (2020).

77. Coupé, P., Manjón, J. V., Lanuza, E. & Catheline, G. Lifespan Changes of the Human Brain In Alzheimer's Disease. *Scientific Reports* **9**, 1–12 (2019).

78. Planche, V. *et al.* Evolution of brain atrophy subtypes during aging predicts long-term cognitive decline and future Alzheimer's clinical syndrome. *Neurobiology of Aging* **79**, 22–29 (2019).

79. Goubran, M. *et al.* Hippocampal segmentation for brains with extensive atrophy using three-dimensional convolutional neural networks. *Human Brain Mapping* **41**, 291–308 (2020).

80. Wang, Z. I. *et al.* Automated MRI volumetric analysis in patients with rasmussen syndrome. *American Journal of Neuroradiology* **37**, 2348–2355 (2016).

81. Skjøth-Rasmussen, J., Jespersen, B. & Brennum, J. The use of Brainsuite iCT for frame-based stereotactic procedures. *Acta Neurochirurgica* **157**, 1437–1440 (2015).

82. Ou, Y. *et al.* Field of View Normalization in Multi-Site Brain MRI. *Neuroinformatics* **16**, 431–444 (2018).

83. D'Andrea, G. *et al.* Intraoperative DTI and brain mapping for surgery of neoplasm of the motor cortex and the corticospinal tract: Our protocol and series in BrainSUITE. *Neurosurgical Review* **35**, 401–412 (2012).

84. Mikhael, S. S. & Pernet, C. A controlled comparison of thickness, volume and surface areas from multiple cortical parcellation packages. *BMC Bioinformatics* **20**, 1–12 (2019).

85. Mikhael, S., Hoogendoorn, C., Valdes-Hernandez, M. & Pernet, C. A critical analysis of neuroanatomical software protocols reveals clinically relevant differences in parcellation schemes. *NeuroImage* **170**, 348–364 (2018).

86. Carass, A. *et al.* Comparing fully automated state-of-the-art cerebellum parcellation from magnetic resonance images. *NeuroImage* **183**, 150–172 (2018).

87. Schwarz, C. G. *et al.* A large-scale comparison of cortical thickness and volume methods for measuring Alzheimer's disease severity. *NeuroImage: Clinical* **11**, 802–812 (2016).

88. Jack, C. R. *et al.* Introduction to the recommendations from the National Institute on Aging-Alzheimer's Association workgroups on diagnostic guidelines for Alzheimer's disease. *Alzheimer's and Dementia* **7**, 257–262 (2011).

89. Albert, M. S. *et al.* The diagnosis of mild cognitive impairment due to Alzheimer's disease: Recommendations from the National Institute on Aging-Alzheimer's Association workgroups on diagnostic guidelines for Alzheimer's disease. *Alzheimer's and Dementia* **7**, 270–279 (2011).

90. Anderson, V. M. *et al.* Gray matter atrophy rate as a marker of disease progression in AD. *Neurobiology of Aging* **33**, 1194–1202 (2012).

91. Boutet, C. *et al.* Detection of volume loss in hippocampal layers in Alzheimer's disease using 7 T MRI: A feasibility study. *NeuroImage: Clinical* **5**, 341–348 (2014).

92. Adler, D. H. *et al.* Characterizing the human hippocampus in aging and Alzheimer's disease using a computational atlas derived from ex vivo MRI and histology. *Proceedings of the National Academy of Sciences of the United States of America* **115**, 4252–4257 (2018).

93. Kwak, K., Niethammer, M., Giovanello, K. S., Styner, M. & Dayan, E. The contribution of hippocampal subfields to the progression of neurodegeneration. *bioRxiv* (2020) doi:10.1101/2020.05.06.081034.

94. Lace, G. *et al.* Hippocampal tau pathology is related to neuroanatomical connections: An ageing population-based study. *Brain* **132**, 1324–1334 (2009).

95. Delgado-González, J. C. *et al.* Neuronal volume of the hippocampal regions in ageing. *Journal of Anatomy* 1–10 (2020) doi:10.1111/joa.13189.

96. Parker, T. D. *et al.* Differences in hippocampal subfield volume are seen in phenotypic variants of early onset Alzheimer's disease. *NeuroImage: Clinical* **21**, 101632 (2019).

97. Carlesimo, G. A. *et al.* Atrophy of presubiculum and subiculum is the earliest hippocampal anatomical marker of Alzheimer's disease. *Alzheimer's and Dementia: Diagnosis, Assessment and Disease Monitoring* **1**, 24–32 (2015).

98. Rössler, M., Zarski, R., Bohl, J. & Ohm, T. G. Stage-dependent and sector-specific neuronal loss in hippocampus during alzheimer's disease. *Acta Neuropathologica* **103**, 363–369 (2002).

99. Braak, E. & Braak, H. Alzheimer's disease: Transiently developing dendritic changes in pyramidal cells of sector CA1 of the Ammon's horn. *Acta Neuropathologica* **93**, 323–325 (1997).

100. Su, L. *et al.* Hippocampal Stratum Radiatum, Lacunosum, and Moleculare Sparing in Mild Cognitive Impairment. *Journal of Alzheimer's Disease* **61**, 415–424 (2018).

101. Dounavi, M. E. *et al.* Volumetric alterations in the hippocampal subfields of subjects at increased risk of dementia. *Neurobiology of Aging* **91**, 36–44 (2020).

102. Zhao, W. *et al.* Trajectories of the hippocampal subfields atrophy in the alzheimer's disease: A structural imaging study. *Frontiers in Neuroinformatics* **13**, 1–9 (2019).

103. Khlif, M. S. *et al.* A comparison of automated segmentation and manual tracing in estimating hippocampal volume in ischemic stroke and healthy control participants. *NeuroImage: Clinical* **21**, (2019).

104. Tang, X., Holland, D., Dale, A. M., Younes, L. & Miller, M. I. Shape abnormalities of subcortical and ventricular structures in mild cognitive impairment and Alzheimer's disease: Detecting, quantifying, and predicting. *Human Brain Mapping* **35**, 3701–3725 (2014).

105. Yi, H. A. *et al.* Relation between subcortical grey matter atrophy and conversion from mild cognitive impairment to Alzheimer's disease. *Journal of Neurology, Neurosurgery and Psychiatry* **87**, 425–432 (2016).

106. Tullo, S. *et al.* MR-based age-related effects on the striatum, globus pallidus, and thalamus in healthy individuals across the adult lifespan. *Human Brain Mapping* **40**, 5269–5288 (2019).

107. Mufson, E. J. *et al.* Mild cognitive impairment: Pathology and mechanisms. *Acta Neuropathologica* **123**, 13–30 (2012).

108. Dicks, E., van der Flier, W. M., Scheltens, P., Barkhof, F. & Tijms, B. M. Single-subject grey matter networks predict future cortical atrophy in preclinical Alzheimer's disease. *Neurobiology of Aging* (2020) doi:10.1016/j.neurobiolaging.2020.05.008.

109. Grothe, M. *et al.* Reduction of basal forebrain cholinergic system parallels cognitive impairment in patients at high risk of developing alzheimer's disease. *Cerebral Cortex* **20**, 1685–1695 (2010).

110. Muth, K. *et al.* Mild Cognitive Impairment in the Elderly is Associated with Volume Loss of the Cholinergic Basal Forebrain Region. *Biological Psychiatry* **67**, 588–591 (2010).

111. Grothe, M., Heinsen, H. & Teipel, S. Longitudinal measures of cholinergic forebrain atrophy in the transition from healthy aging to Alzheimer's disease. *Neurobiology of Aging* **34**, 1210–1220 (2013).

112. Ossenkoppele, R. *et al.* Associations between tau, Aβ, and cortical thickness with cognition in Alzheimer disease. *Neurology* **92**, e601–e612 (2019).

113. Barber, R., McKeith, I., Ballard, C. & O'Brien, J. Volumetric MRI study of the caudate nucleus in patients with dementia with Lewy bodies, Alzheimer's disease, and vascular dementia. *Journal of Neurology Neurosurgery and Psychiatry* **72**, 406–407 (2002).

114. Yan, T. *et al.* Early-Stage Identification and Pathological Development of Alzheimer's Disease Using Multimodal MRI. *Journal of Alzheimer's Disease* **68**, 1013–1027 (2019).

115. Botzung, A., Philippi, N., Noblet, V., Loureiro De Sousa, P. & Blanc, F. Pay attention to the basal ganglia: A volumetric study in early dementia with Lewy bodies. *Alzheimer's Research and Therapy* **11**, 1–9 (2019).

116. Sun, N., Mormino, E. C., Chen, J., Sabuncu, M. R. & Yeo, B. T. T. Multi-modal latent factor exploration of atrophy, cognitive and tau heterogeneity in Alzheimer's disease. *NeuroImage* **201**, (2019).

117. Young, A. L. *et al.* Uncovering the heterogeneity and temporal complexity of neurodegenerative diseases with Subtype and Stage Inference. *Nature Communications* **9**, 1–16 (2018).

118. Noh, Y. *et al.* Anatomical heterogeneity of Alzheimer disease Based on cortical thickness on MRIs. *Neurology* **83**, 1936–1944 (2014).

119. Ferreira, D. *et al.* Distinct subtypes of Alzheimer's disease based on patterns of brain atrophy: Longitudinal trajectories and clinical applications. *Scientific Reports* **7**, 1–13 (2017).

120. Gorno-Tempini, M. L. *et al.* Classification of primary progressive aphasia and its variants. *Neurology* **76**, 1006–1014 (2011).

121. Phillips, J. S. *et al.* Tau PET imaging predicts cognition in atypical variants of Alzheimer's disease. *Human Brain Mapping* **39**, 691–708 (2018).

122. Ossenkoppele, R. *et al.* The behavioural/dysexecutive variant of Alzheimer's disease: Clinical, neuroimaging and pathological features. *Brain* **138**, 2732–2749 (2015).

123. Ossenkoppele, R. *et al.* Tau PET patterns mirror clinical and neuroanatomical variability in Alzheimer's disease. *Brain* **139**, 1551–1567 (2016).

124. Arbabshirani, M. R., Plis, S., Sui, J. & Calhoun, V. D. Single subject prediction of brain disorders in neuroimaging: Promises and pitfalls. *NeuroImage* **145**, 137–165 (2017).

125. Spires-Jones, T. L. & Hyman, B. T. The Intersection of Amyloid Beta and Tau at Synapses in Alzheimer's Disease. *Neuron* **82**, 756–771 (2014).

126. McKhann, G. M. *et al.* The diagnosis of dementia due to Alzheimer's disease: Recommendations from the National Institute on Aging-Alzheimer's Association workgroups on diagnostic guidelines for Alzheimer's disease. *Alzheimer's and Dementia* **7**, 263–269 (2011).

127. Sørensen, L. *et al.* Early detection of Alzheimer's disease using MRI hippocampal texture. *Human Brain Mapping* **37**, 1148–1161 (2016).

128. McEvoy, L. K. & Brewer, J. B. Quantitative structural MRI for early detection of Alzheimers disease. *Expert Review of Neurotherapeutics* **10**, 1675–1688 (2010).

129. Fotuhi, M., Do, D. & Jack, C. Modifiable factors that alter the size of the hippocampus with ageing. *Nature Reviews Neurology* **8**, 189–202 (2012).

130. Erickson, K. I. *et al.* Exercise training increases size of hippocampus and improves memory. *Proceedings of the National Academy of Sciences* **108**, 3017–3022 (2011).

131. Varma, V. R., Chuang, Y. F., Harris, G. C., Tan, E. J. & Carlson, M. C. Low-intensity daily walking activity is associated with hippocampal volume in older adults. *Hippocampus* **25**, 605–615 (2015).

132. Liang, Y., Ryan, N. S., Schott, J. M. & Fox, N. C. Imaging the onset and progression of Alzheimer's disease: Implications for prevention trials. *Journal of Alzheimer's Disease* **33**, (2013).

133. Coupé, P., Eskildsen, S. F., Manjón, J. v., Fonov, V. S. & Collins, D. L. Simultaneous segmentation and grading of anatomical structures for patient's classification: Application to Alzheimer's disease. *NeuroImage* **59**, 3736–3747 (2012).

134. Sperling, R. A. *et al.* Toward defining the preclinical stages of Alzheimer's disease: Recommendations from the National Institute on Aging-Alzheimer's Association workgroups on diagnostic guidelines for Alzheimer's disease. *Alzheimer's and Dementia* **7**, 280–292 (2011).

135. Veitch, D. P. *et al.* Understanding disease progression and improving Alzheimer's disease clinical trials: Recent highlights from the Alzheimer's Disease Neuroimaging Initiative. *Alzheimer's and Dementia* **15**, 106–152 (2019).

136. Vanhoenacker, A. S., Sneyers, B., de Keyzer, F., Heye, S. & Demaerel, P. Evaluation and clinical correlation of practical cut-offs for visual rating scales of atrophy: normal aging versus mild cognitive impairment and Alzheimer's disease. *Acta Neurologica Belgica* **117**, 661–669 (2017).

137. Shaw, T., York, A., Ziaei, M., Barth, M. & Bollmann, S. Longitudinal Automatic Segmentation of Hippocampal Subfields (LASHiS) using Multi-Contrast MRI. *NeuroImage* 116798 (2020) doi:10.1016/j.neuroimage.2020.116798.

138. Scarpazza, C. *et al.* Translating research findings into clinical practice: a systematic and critical review of neuroimaging-based clinical tools for brain disorders. *Translational Psychiatry* **10**, (2020).

139. Henneman, W. J. P. *et al.* Hippocampal atrophy rates in Alzheimer disease: Added value over whole brain volume measures. *Neurology* **72**, 999–1007 (2009).

140. Leung, K. K. *et al.* Automated cross-sectional and longitudinal hippocampal volume measurement in mild cognitive impairment and Alzheimer's disease. *NeuroImage* **51**, 1345–1359 (2010).

141. Frankó, E. & Joly, O. Evaluating Alzheimer's Disease Progression Using Rate of Regional Hippocampal Atrophy. *PLoS ONE* **8**, (2013).

142. Mak, E. *et al.* Longitudinal assessment of global and regional atrophy rates in Alzheimer's disease and dementia with Lewy bodies. *NeuroImage: Clinical* **7**, 456–462 (2015).

143. Eustache, P., Nemmi, F., Saint-Aubert, L., Pariente, J. & Péran, P. Multimodal Magnetic Resonance Imaging in Alzheimer's Disease Patients at Prodromal Stage. *Journal of Alzheimer's Disease* **50**, 1035–1050 (2016).

144. Pagani, M. *et al.* Predicting the transition from normal aging to Alzheimer's disease: A statistical mechanistic evaluation of FDG-PET data. *NeuroImage* **141**, 282–290 (2016).

145. Qiu, S. *et al.* Development and validation of an interpretable deep learning framework for Alzheimer's disease classification. *Brain* 1–14 (2020) doi:10.1093/brain/awaa137.

146. Zhao, W. *et al.* Automated Brain MRI Volumetry Differentiates Early Stages of Alzheimer's Disease From Normal Aging. *Journal of Geriatric Psychiatry and Neurology* **32**, 354–364 (2019).

147. Li, H., Habes, M., Wolk, D. A. & Fan, Y. A deep learning model for early prediction of Alzheimer's disease dementia based on hippocampal magnetic resonance imaging data. *Alzheimer's and Dementia* **15**, 1059–1070 (2019).

148. Bachli, M. B. *et al.* Evaluating the reliability of neurocognitive biomarkers of neurodegenerative diseases across countries: A machine learning approach. *NeuroImage* **208**, (2020).

149. Bouts, M. J. R. J. *et al.* Detection of mild cognitive impairment in a community-dwelling population using quantitative, multiparametric MRI-based classification. *Human Brain Mapping* **40**, 2711–2722 (2019).

150. Forouzannezhad, P. *et al.* A Gaussian-based model for early detection of mild cognitive impairment using multimodal neuroimaging. *Journal of Neuroscience Methods* **333**, 108544 (2020).

151. Khan, R. U., Tanveer, M. & Pachori, R. B. A novel method for the classification of Alzheimer's disease from normal controls using magnetic resonance imaging. *Expert Systems* 1–22 (2020) doi:10.1111/exsy.12566.

152. Oh, K., Chung, Y. C., Kim, K. W., Kim, W. S. & Oh, I. S. Classification and Visualization of Alzheimer's Disease using Volumetric Convolutional Neural Network and Transfer Learning. *Scientific Reports* **9**, 1–16 (2019).

153. Dukart, J. *et al.* Meta-analysis based SVM classification enables accurate detection of Alzheimer's disease across different clinical centers using FDG-PET and MRI. *Psychiatry Research - Neuroimaging* **212**, 230–236 (2013).

154. Lecun, Y., Bengio, Y. & Hinton, G. Deep learning. *Nature* **521**, 436–444 (2015).

Table 1. Comparison between Alzheimer's disease (AD) and healthy controls (HC).

Measure	**Alzheimer's Disease**	**Healthy Control**	***p***
n	22	22	-
Female (n [%])	11 [50]	11 [50]	-
Age (mean [SD])	70.64 [5.55]	70.61 [7.54]	0.916
MMSE (mean [SD]; min-max)	17.272 [5.461]; 5-26	29.087 [1.083]; 27-30	< 0.001

Table 2. Summary of the independent-sample t-tests comparing volumetric data between the participants with Alzheimer's disease and healthy controls and the correlation of the data with MMSE scores using **CAT** method.

	Comparison between groups			**Correlation with MMSE**	
Brain Area	***t***	***p*↑**	***d***	r^2	***p***
Fusiform Gyrus	10.793	< 0.000001*	3.413	0.723	< 0.000001*
Parahippocampus Gyrus	9.936	< 0.000001*	3.142	0.536	< 0.000001*
Hippocampus	9.753	< 0.000001*	3.084	0.460	0.000001*
Entorhinal Cortex	9.717	< 0.000001*	3.073	0.476	< 0.000001*
Amygdala	9.043	< 0.000001*	2.860	0.445	0.000001*
Inferior Temporal Gyrus	8.939	< 0.000001*	2.827	0.653	< 0.000001*
Middle Temporal Gyrus	7.632	< 0.000001*	2.413	0.619	< 0.000001*
Temporal Pole	7.185	< 0.000001*	2.272	0.491	< 0.000001*
Basal Forebrain	6.658	< 0.000001*	2.105	0.453	0.000001*
Thalamus	6.344	< 0.000001*	2.006	0.471	0.000001*
Angular Gyrus	5.808	0.000001*	1.837	0.507	< 0.000001*
Accumbens	5.275	0.000005*	1.668	0.289	0.000236*
Inferior Occipital Gyrus	5.228	0.000006*	1.653	0.527	< 0.000001*
Superior Temporal Gyrus	5.186	0.000007*	1.640	0.513	< 0.000001*
Supramarginal Gyrus	5.101	0.000009*	1.613	0.498	< 0.000001*
Anterior Insula	4.955	0.000014*	1.567	0.346	0.000043*
Occipital Fusiform Gyrus	4.519	0.000054*	1.429	0.472	0.000001*
Middle Occipital Gyrus	4.515	0.000055*	1.428	0.417	0.000004*
Posterior Insula	4.447	0.000068*	1.406	0.338	0.000054*
Planum Polare	4.232	0.000131*	1.338	0.349	0.000038*
Anterior Cingulate Gyrus	4.225	0.000134*	1.336	0.362	0.000025*
Superior Parietal Lobule	4.131	0.000179*	1.306	0.423	0.000003*
Caudate	3.959	0.000301*	1.252	0.234	0.001155
Subcallosal Area	3.847	0.000420*	1.217	0.299	0.000180*
Middle Frontal Gyrus	3.796	0.000490*	1.200	0.328	0.000073*
Medial Orbital Gyrus	3.739	0.000579*	1.182	0.278	0.000331*
Inferior Frontal Gyrus	3.691	0.000666*	1.167	0.373	0.000017*
Precuneus	3.633	0.000788*	1.149	0.349	0.000038*
Superior Medial Frontal Gyrus	3.543	0.001023	1.120	0.312	0.000120*
Putamen	3.525	0.001077	1.115	0.203	0.002822
Temporal	3.489	0.001195	1.103	0.340	0.000051*

Anterior Orbital Gyrus	3.413	0.001484	1.079	0.244	0.000894
Posterior Orbital Gyrus	3.272	0.002203	1.035	0.255	0.000643*
Lingual Gyrus	3.263	0.002262	1.032	0.304	0.000158*
Posterior Cingulate Gyrus	3.226	0.002506	1.020	0.314	0.000117*
Central Operculum	3.116	0.003388	0.985	0.372	0.000018*
Frontal Operculum	2.999	0.004638	0.948	0.265	0.000479*
Supplementary Motor Cortex	2.969	0.005032	0.939	0.310	0.000128*
Exterior Cerebellum	2.934	0.005513	0.928	0.163	0.007986
Superior Frontal Gyrus	2.870	0.006523	0.908	0.199	0.003066
Parietal Operculum	2.864	0.006637	0.906	0.320	0.000095*
Middle Cingulate Gyrus	2.734	0.009272	0.865	0.269	0.000432*
Gyrus Rectus	2.660	0.011190	0.841	0.143	0.013603
Optic Chiasm	2.531	0.015401	0.800	0.066	0.101456
Lateral Orbital Gyrus	2.427	0.019841	0.767	0.158	0.009194
Temporal Transverse Gyrus	2.345	0.024056	0.742	0.189	0.003960
Superior Occipital Gyrus	2.290	0.027347	0.724	0.245	0.000849
Medial Precentral Gyrus	2.250	0.030015	0.712	0.196	0.003321
Cuneus	2.091	0.042968	0.661	0.187	0.004135
Inferior Frontal Orbital Gyrus	2.063	0.045679	0.652	0.123	0.022887
Postcentral Gyrus	1.687	0.099402	0.533	0.142	0.013747
Frontal Pole	1.603	0.116854	0.507	0.067	0.098513
Occipital Pole	1.596	0.118311	0.505	0.127	0.020199
Inferior Frontal Angular Gyrus	1.518	0.136864	0.480	0.134	0.017041
Cerebellum White Matter	1.319	0.194795	0.417	0.079	0.071875
Precentral Gyrus	1.196	0.238644	0.378	0.124	0.022441
Medial Postcentral Gyrus	1.061	0.294904	0.336	0.070	0.090174
Brainstem	-0.875	0.386852	0.277	0.005	0.640175
Cerebellar Vermal Lobules VI-VII	0.699	0.488487	0.221	0.024	0.325448
Cerebellar Vermal Lobules VIII-X	0.617	0.541029	0.195	0.015	0.434774
Cerebellar Vermal Lobules I-V	0.218	0.828189	0.069	0.016	0.430517
Globus Pallidus	-0.212	0.832833	0.067	0.001	0.860265
Calcarine Cortex	0.198	0.843964	0.063	0.013	0.473158

Notes: ↑ rows are sorted based on the *p* values for the t-test; * $p < 0.000793$ Bonferroni corrected for multiple comparison; *d* represents Cohen's d effect size; MMSE: mini mental state examination

Table 3. Summary of the independent-sample t-tests comparing volumetric data between the participants with Alzheimer's disease and healthy controls and the correlation of the data with MMSE scores using **volBrain** method.

	Comparison between groups			**Correlation with MMSE**	
Brain Area	***t***	***p*↑**	***d***	r^2	***p***
Amygdala	10.217	< 0.000001*	3.231	0.428	0.000001*
Hippocampus	6.58	< 0.000001*	2.081	0.256	0.000395*
Accumbens	5.813	0.000001*	1.838	0.339	0.000027*
Thalamus	4.422	0.000065*	1.398	0.317	0.000057*
Caudate	4.149	0.000154*	1.312	0.169	0.005091
Cerebellum	2.063	0.045216	0.652	0.094	0.041135
Globus Pallidus	-1.103	0.276245	0.349	0.026	0.287427
Putamen	0.846	0.402030	0.268	0.019	0.366267

Notes: ↑ rows are sorted based on the *p* values for the t-test; * $p < 0.0038$ Bonferroni corrected for multiple comparison; *d* represents Cohen's d effect size; MMSE: mini mental state examination;

Table 4. Summary of the independent-sample t-tests comparing volumetric data between the participants with Alzheimer's disease and healthy controls and the correlation of the data with MMSE scores using **BrainSuite** segmentation method.

	Comparison between groups			**Correlation with MMSE**	
Brain Area	**t**	**p↑**	**d**	**r2**	**p**
Inferior Temporal Gyrus	7.245	< 0.000001*	2.184	0.677	0.000001*
Middle Temporal Gyrus	4.738	0.000029*	1.429	0.697	< 0.000001*
Third Ventricle	-4.354	0.000094*	1.313	-0.522	0.000468*
Superior Temporal Gyrus	3.944	0.000323*	1.189	0.507	0.000722*
Supramarginal Gyrus	3.698	0.000668*	1.115	0.509	0.000683*
Angular Gyrus	3.632	0.000809*	1.095	0.52	0.000498*
Middle Occipital Gyrus	3.543	0.001043	1.068	0.536	0.000303*
Pars Opercularis	2.958	0.005237	0.892	0.45	0.003137
Inferior Occipital Gyrus	2.663	0.011206	0.803	0.383	0.013402
Accumbens	-2.64	0.011866	0.796	-0.481	0.001457
Superior Parietal Gyrus	2.534	0.015392	0.764	0.434	0.004538
Superior Colliculus	-2.532	0.015481	0.763	-0.338	0.030512
Parahippocampal Gyrus	2.447	0.019029	0.738	0.428	0.005294
Cingulate Gyrus	-2.374	0.022629	0.716	-0.356	0.022147
Fusiform Gyrus	2.269	0.028864	0.684	0.155	0.334311
Insula	2.133	0.039251	0.643	0.255	0.107583
Globus Pallidus	-1.995	0.053041	0.602	-0.231	0.146663
Cerebellum	1.979	0.054949	0.597	0.191	0.232289
Basal Forebrain	-1.909	0.063590	0.576	-0.243	0.126172
Anterior Orbito-Frontal Gyrus	1.856	0.070973	0.560	0.234	0.140158
Subcallosal Gyrus	-1.847	0.072330	0.557	-0.207	0.194909
Pars Orbitalis	1.82	0.076458	0.549	0.275	0.081327
Lingual Gyrus	-1.809	0.078196	0.545	-0.316	0.043952
Middle Frontal Gyrus	1.807	0.078496	0.545	0.284	0.071904
Lateral Geniculate Nucleus	1.78	0.082929	0.537	0.253	0.109970
Middle Orbito-Frontal Gyrus	1.744	0.089100	0.526	0.142	0.374241
Temporal Pole	1.591	0.119752	0.480	0.022	0.892295
Post-Central Gyrus	1.501	0.141345	0.453	0.315	0.044533
Hippocampus	-1.241	0.221958	0.374	-0.162	0.311495
Transverse Temporal Gyrus	1.138	0.261864	0.343	0.268	0.090858
Transvers Frontal Gyrus	1.099	0.278660	0.331	0.272	0.085861

Thalamus	0.968	0.339074	0.292	0.087	0.586936
Inferior Colliculus	0.94	0.352768	0.283	0.102	0.526091
Pars Triangularis	0.911	0.367812	0.275	0.216	0.174328
Claustrum	0.87	0.389785	0.262	0.163	0.308227
Caudate	-0.863	0.393478	0.260	-0.122	0.448542
Pre-Central Gyrus	0.859	0.395408	0.259	0.242	0.128116
Paracentral Lobule	0.858	0.395895	0.259	0.128	0.424284
Superior Occipital Gyrus	0.858	0.395943	0.259	0.169	0.291590
Cuneus	0.843	0.404153	0.254	0.106	0.510235
Putamen	0.653	0.517714	0.197	-0.001	0.995473
Lateral Orbitofrontal Gyrus	-0.548	0.586738	0.165	-0.071	0.658410
Gyrus Rectus	-0.516	0.608533	0.156	-0.123	0.442668
Medial Geniculate Nucleus	-0.505	0.616072	0.152	-0.122	0.448980
Mamillary Body	0.492	0.625193	0.148	0.125	0.436896
Precuneus	-0.49	0.627078	0.148	-0.007	0.967476
Posterior Orbito-Frontal Gyrus	0.445	0.658856	0.134	0.02	0.901794
Brainstem	0.209	0.835439	0.063	-0.015	0.925512
Superior Frontal Gyrus	0.202	0.840699	0.061	0.132	0.411455
Amygdala	0.145	0.885584	0.044	-0.109	0.497327

Notes: ↑ rows are sorted based on the *p* values for the t-test; * $p < 0.001000$ Bonferroni corrected for multiple comparison; *d* represents Cohen's d effect size; MMSE: mini mental state examination

Table 5. Summary of the independent-sample t-tests comparing volumetric data between the participants with Alzheimer's disease and healthy controls and the correlation of the data with MMSE scores using **HIPS** segmentation method.

	Comparison between groups			**Correlation with MMSE**	
Brain Area	***t***	***p*↑**	***d***	r^2	***p***
SR-SL-SM	8.990	< 0.000001*	2.843	0.393	0.000004*
Hippocampus	8.619	< 0.000001*	2.726	0.388	0.000005*
CA4/Dentate Gyrus	8.248	< 0.000001*	2.608	0.402	0.000003*
CA1	6.308	< 0.000001*	1.995	0.256	0.000389*
Subiculum	5.121	0.000007*	1.619	0.229	0.000873*
CA2-CA3	5.025	0.000009*	1.589	0.288	0.000142*

Notes: ↑ rows are sorted based on the *p* values for the t-test; * $p < 0.008333$ Bonferroni corrected for multiple comparison; *d* represents Cohen's d effect size; MMSE: mini mental state examination; SR-SL-SM: strata radiatum/lacunosum/moleculare

Table 6. Correlation of the size of common brain areas reported by the three segmentation methods

		CAT		volBrain	
	Brain Area	r^2	p	r^2	p
BrainSuite	Accumbens	-0.227	0.159813	-0.277	0.078996
	Amygdala	0.240	0.136249	0.029	0.858460
	Caudate	0.169	0.298015	0.090	0.577545
	Globus Pallidus	-0.118	0.469153	0.184	0.249666
	Hippocampus	-0.162	0.318747	-0.275	0.081327
	Putamen	0.328	0.039077	-0.186	0.243349
	Thalamus	0.188	0.245249	0.177	0.268448
volBrain	Accumbens	0.633	0.000007*		
	Amygdala	0.632	0.000007*		
	Caudate	0.470	0.001678*		
	Globus Pallidus	-0.245	0.118543		
	Hippocampus	0.637	0.000006*		
	Putamen	0.020	0.898315		
	Thalamus	0.541	0.000214*		

Notes: * $p < 0.002380$ Bonferroni corrected for multiple comparison

Figures' Caption

Figure 1. Processing pipeline for volBrain and HIPS adapted from Manjón and Coupé (2016) [34] under the terms of the Creative Commons Attribution License (CC BY).

Figure 2. Processing pipeline for CAT

Figure 3. Processing pipeline for BrainSuite

Figure 4. Subcortical structures in an AD patient and a HC participant using CAT segmentation method. The histograms show the volume of each brain area

Figure 5. Cerebellum MRI-T1 brain segmentation in an AD patient and a HC participant using volBrain segmentation method.

Figure 6. Cerebellum MRI-T1 brain segmentation in an AD patient and a HC participant using BrainSuite segmentation method.

Figure 7. Left and right hippocampus subfield segmentation in an AD patient and a HC participant

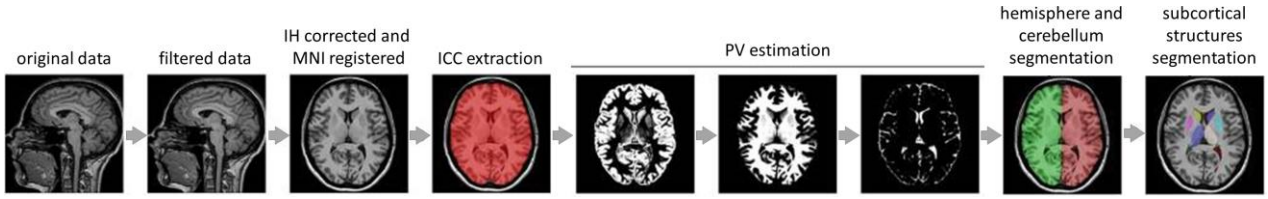

Figure 1. Processing pipeline for volBrain and HIPS adapted from Manjón and Coupé (2016) [34] under the terms of the Creative Commons Attribution License (CC BY).

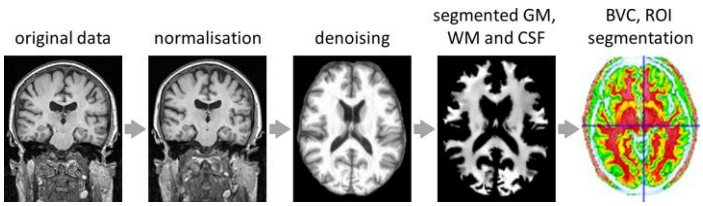

Figure 2. Processing pipeline for CAT.

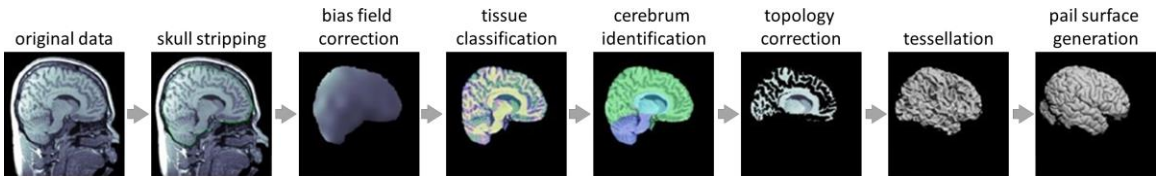

Figure 3. Processing pipeline for BrainSuite.

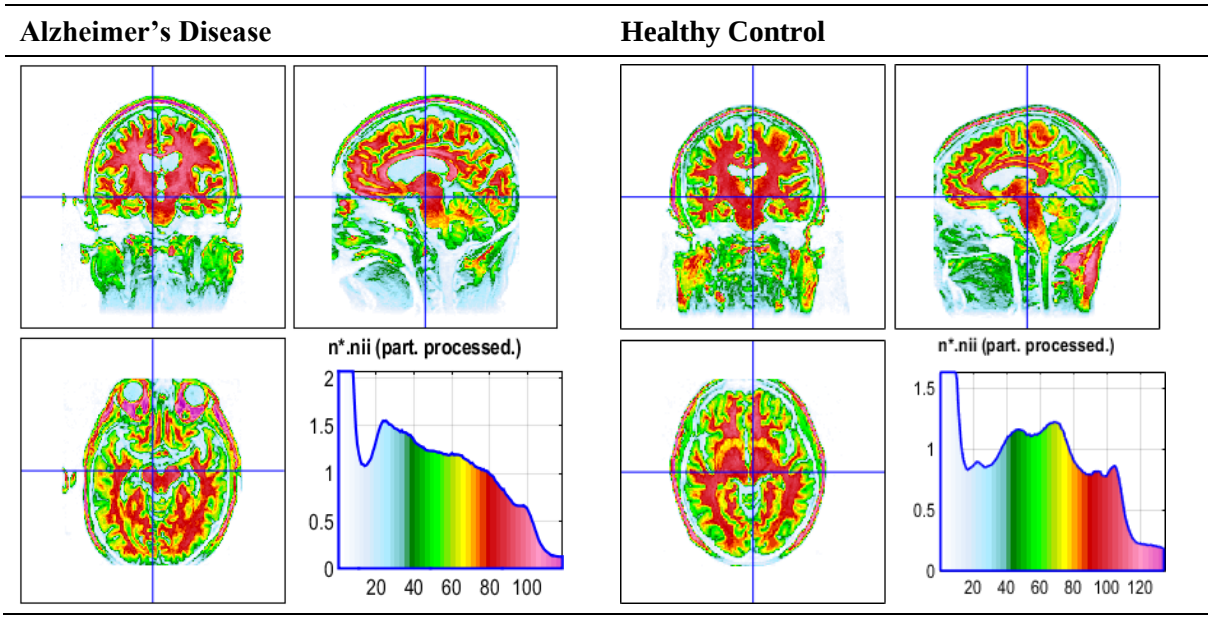

Figure 4. Subcortical structures in an AD patient and a HC participant using CAT segmentation method. The histograms show the volume of each brain area.

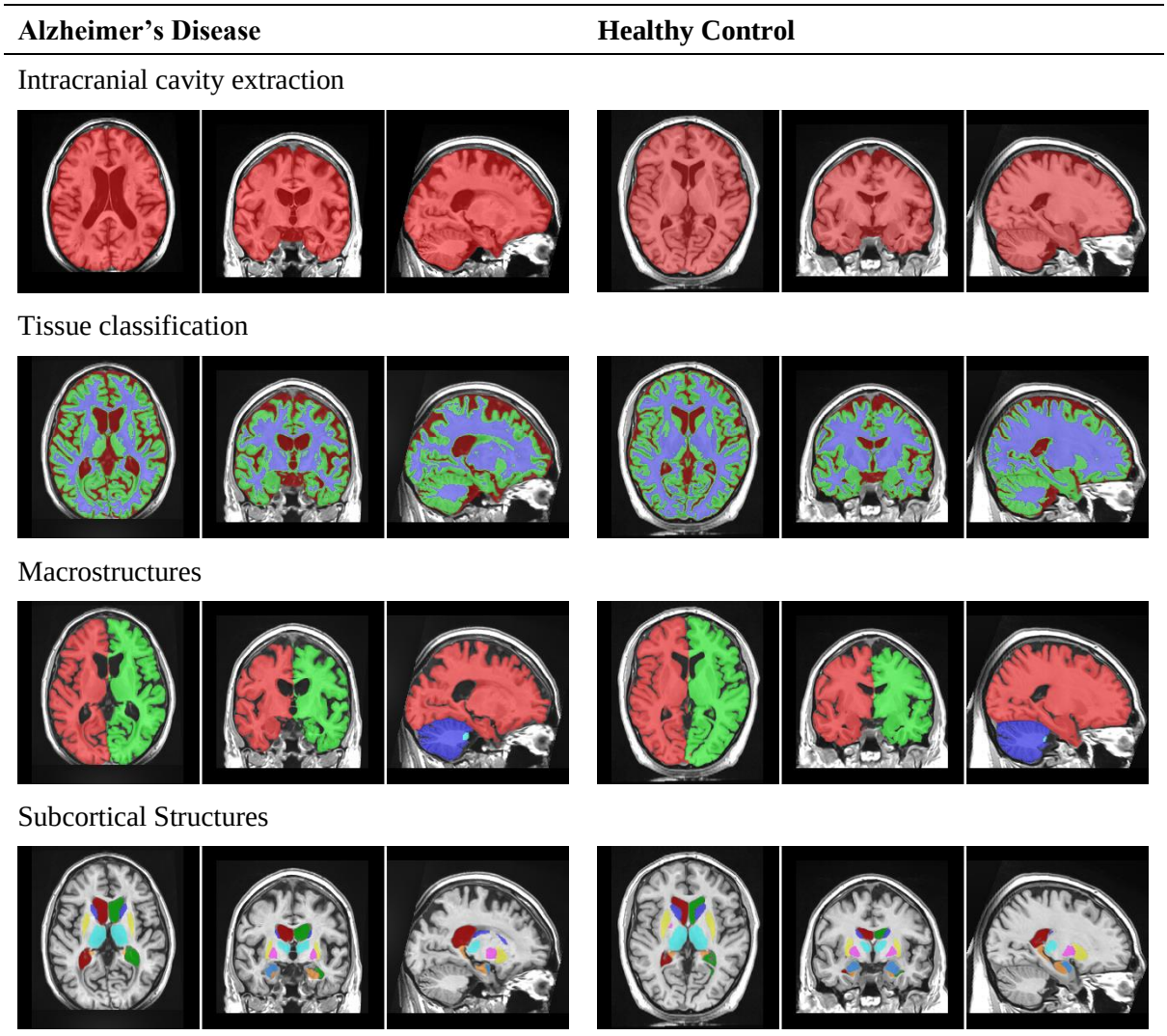

Figure 5. Cerebellum MRI-T1 brain segmentation in an AD patient and a HC participant using volBrain segmentation method.

Alzheimer's Disease	**Healthy Control**
inner cortex segmentation	
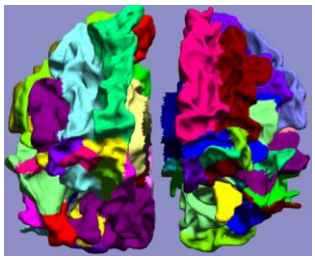	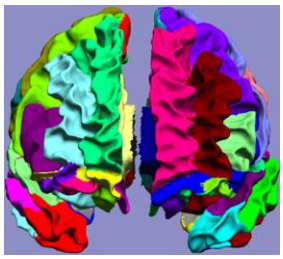
pail cortex segmentation	
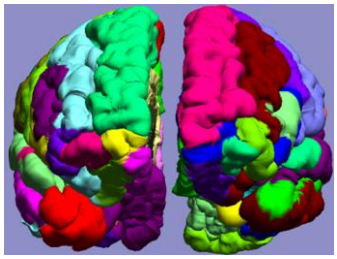	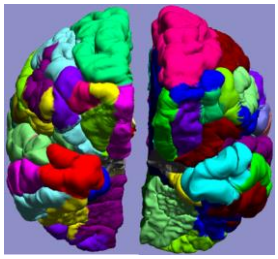

Figure 6. Cerebellum MRI-T1 brain segmentation in an AD patient and a HC participant using BrainSuite segmentation method.

Alzheimer's Disease	**Healthy Control**
Left Hippocampus	
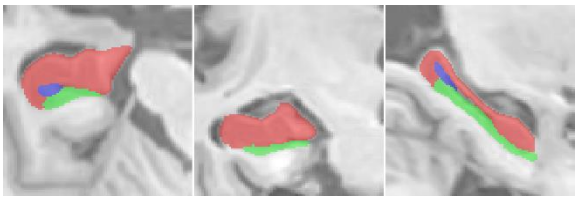	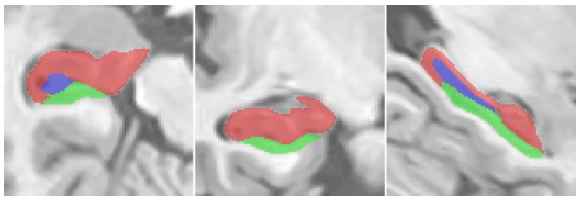
Right Hippocampus	
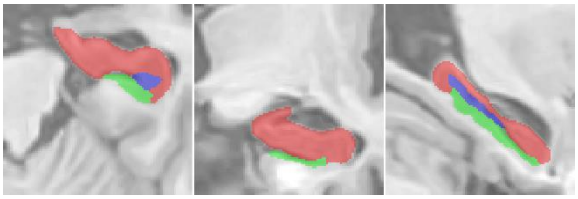	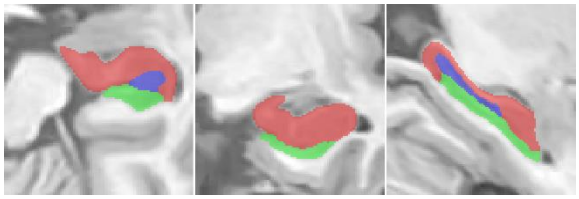

Figure 7. Left and right hippocampus subfield segmentation in an AD patient and a HC participant using HIPS segmentation method.